CrossMark

Fabrication of carbon nanotube/cobalt oxide nanocomposites via electrophoretic deposition for supercapacitor electrodes

Nagesh Kumar[1] · Yun-Cheng Yu[1] · Yi Hsuan Lu[1] · Tseung Yuen Tseng[1]

Abstract The cobalt oxide and carbon nanotubes (Co_3O_4/CNTs) nanocomposites are successfully synthesized using hydrothermal method. The as-synthesized nanocomposite materials are utilized in the electrophoretic deposition (EPD) to fabricate the electrodes, whose electrochemical properties are investigated in a three-electrode configuration cell with 1 M KOH electrolyte. By adjusting the precursor concentration, reaction time in hydrothermal process, and annealing temperature, the optimum conditions are obtained. From the experimental results, when the cobalt nitrate concentration is taken as 2 mmol, reaction time is 8 h, and the temperature is maintained at 180 °C in the hydrothermal process, the synthesized Co_3O_4/CNTs nanocomposites shows the highest specific capacitance of 705 F g^{-1} at a charging current of 3 A g^{-1}. Besides, the binder-free electrode preparation through EPD has effectively reduced the inner resistance of the electrode and makes the cycle stability excellent.

Introduction

In recent years, the issues of energy storage and energy conversion draw much more attention with the fast development of technology industry. However, in modern society we people mainly rely on the chemical energy stored in the fossil fuels due to availability on demand at relatively low cost, which further induced other serious problems such as the depletion of fossil fuels and global warming created by combustion of fossil fuels.

As a result, the first priority is to develop a high-performance, low-cost, and environmentally friendly energy storage device such as supercapacitors (SCs, also called electrochemical capacitors or ultra capacitors), battery modules (especially lithium-ion batteries), and fuel cells [1]. The SCs are considered to be a potential candidate due to their outstanding power density, rapid charge/discharge rates, long life expectancy, and green environmental protection [2]. Although there are many advantages as mentioned above, yet there are still lots of challenges to overcome [3]. Currently, researches in SCs are focused on increasing their energy densities and decreasing their overall production costs by finding suitable electrode materials and manufacturing method.

Generally, SCs are classified into two categories depending on their charge storage mechanism. One is electric double-layer capacitors (EDLCs), in which charges are stored via ion absorption/desorption process at the electrode–electrolyte interfaces and no chemical reactions involved; the other group is called pseudocapacitors or faradic SCs, in which charges are stored through fast, reversible redox reactions. Generally, two different charge storage mechanisms coexist in a supercapacitor system. But in a particular system one storage mechanism occupies the leading position and the other is relatively weak [4]. Moreover, it has been generally accepted that the EDLCs have higher power density, while faradic SCs possess higher specific capacitance and higher energy density [5, 6]. For various practical applications, it is necessary to develop the SCs with both high power density and high energy density. To achieve such a goal, hybrid capacitors, which consist of the materials used in EDLCs and faradic SCs, have been extensively investigated in order to

✉ Tseung Yuen Tseng
  tseng@cc.nctu.edu.tw

[1] Department of Electronics Engineering and Institute of Electronics, National Chiao Tung University, Hsinchu 300, Taiwan

combine the excellent properties of both SCs. The electric double-layer capacitors are based on carbon materials, while the faradic pseudocapacitors rely on metal oxides and conducting polymers. However, the CNTs/conducting polymer electrodes do not have long cycle life due to the degradation of polymers [7]. Transition-metal oxides attached to CNTs are expected to have high specific capacitance and good rate capability [8]. Cobalt oxides with low cost, natural abundance, and environment safety have been considered the promising electrode materials for supercapacitor applications. These can interact with electrolyte ions not only at the surface, but also throughout the bulk [9]. However, the charge transfer reaction kinetics is limited due to their poor conductivity and difficulty in the penetration of electrolyte ions into these [10]. Therefore, for a cobalt oxide electrode, we need to improve its electrical conductivity and increase its specific surface area. In this regard, carbon nanotubes (CNTs) are attractive materials due to their unique one-dimensional mesoporous structure, highly accessible surface area, good conductivity, and high chemical stability [11]. Recently, supercapacitive properties of several Co_3O_4/carbonaceous composite-like systems have been investigated [12–16]. It has been concluded that electrochemical properties of such systems strongly depend on synthesis parameters and electrode fabrication techniques. Hydrothermal technique is well suited for the synthesis of metal oxide–carbon composite materials with high crystallinity and narrow particle size distribution. In basic hydrothermal process, the starting chemicals in water or other solvents are heated in a high-pressure reactor at an elevated temperature. At high pressure, the solubility of reactants increases and the desired material can be synthesized even at low temperatures, which in turn suppresses the particle grain growth. We can easily control hydrothermal time to synthesize Co_3O_4/CNTs nanocomposites with various morphologies. Several techniques [e.g., slurry method, vacuum filtration, paste/press technique, and electrophoretic deposition (EPD)] have been developed to fabricate electrodes for supercapacitors [17–20]. Among these techniques, electrophoretic deposition is the most preferable for electrode fabrication for the practical application of pseudocapacitor due to its low cost, fast room-temperature processing, easy control over the mass of the deposited particles, binder-free nature, and suitability for mass production.

In the present work, high-performance binder-free porous network Co_3O_4/CNTs nanocomposite electrodes for SC applications have been fabricated using hydrothermal and one-step EPD methods. The nanocomposite synthesis method, electrode fabrication technique, and improved electrochemical performance of Co_3O_4/CNTs nanocomposite have been discussed thoroughly. The effects of different hydrothermal reaction times and cobalt nitrate concentrations on the electrochemical properties of Co_3O_4/CNT nanocomposite electrodes have been monitored. The supercapacitor material synthesized in a hydrothermal reaction for 8 h using 2 mmol cobalt nitrate concentration shows high specific capacitance (705 F g^{-1} at a current density of 3 A g^{-1}) and exhibits excellent cycling stability with ∼125 % capacitance retention after 10,000 charge/discharge cycles.

Experimental

Nickel foil acid treatment

For electrochemical analysis, testing composite material was directly deposited on Ni substrate via EPD technique. Before that, nickel foil was cleaned by ultrasonic agitation in ethanol for 10 min and dried in an oven at 100 °C. After that, it was etched with 10 % nitric acid solution for 30 min, washed thoroughly with deionized (DI) water using an ultrasonic bath, and dried in an oven at 100 °C for 12 h.

Carbon nanotube purification

In order to remove some catalysts like Fe, Co, and Ni and to obtain competent defects on the wall of CNTs, which increase the adsorption site on the surface, the commercial CNTs (specific surface area: 40–300 m^2 g^{-1}, length: 5–20 μm) were purified by dissolving them in a boiling 70 % nitric acid solution for 24 h. After washing with plenty of DI water, the acid-treated CNTs were dried in an oven at 100 °C for further use in synthesizing Co_3O_4/CNTs nanocomposites.

Synthesis of Co_3O_4/CNTs nanocomposites

Co_3O_4/CNTs nanocomposites were synthesized by hydrothermal method. A total of 0.58 g of $Co(NO_3)_2 \cdot 6H_2O$ was dissolved in a solution containing 18 mL of DI water and 18 mL of methanol to form a reddish solution. After 30 min of stirring, 0.3 g of urea was added into it and the resultant solution was further stirred for 1 h. Subsequently, 24 mg of acid-treated CNTs were dispersed in this solution via ultrasonication, and 0.2 M NaOH solution was then added drop by drop to form hydroxide precipitate. The final solution was transferred into a 50-mL Teflon-lined sealed stainless steel autoclave and maintained at 180 °C under autogenous pressure for different hydrothermal times (1, 4, 8, 12, and 16 h). After reaction, the autoclave was allowed to cool down naturally and the obtained material was rinsed with DI water until pH of the washing solution reached ∼7. The resulting material was dried in air at 100 °C for 12 h to obtain cobalt oxide/CNTs nanocomposites.

Preparation of electrodes

To prepare working electrodes, Co_3O_4/CNTs nanocomposites were deposited on the etched and cleaned Ni substrate (10 mm × 30 mm × 1 mm) via EPD. The electrolyte used in EPD was a suspension of 0.03 g Co_3O_4/CNTs nanocomposite in 40 mL isopropyl alcohol containing 0.4 mL 37 % HCl. Before EPD, nanocomposite powder was dispersed well in the electrolyte solution via ultrasonic agitation for 30 min.

For EPD, the nickel and platinum substrates were placed in the electrolyte solution at a distance of 1 cm apart and used as cathode and anode electrodes, respectively. The Co_3O_4/CNTs nanocomposites were electrophoretically deposited on the nickel substrate after applying a constant voltage of 50 V for 2 min using DC power supply. A film composed of Co_3O_4/CNTs nanocomposites was then obtained after drying in an oven at 100 °C for 12 h. The loading of nanocomposites film on Ni substrate was about 97.5 μg as weighed by the microbalance (PRECISA XR125SM-FR) with an accuracy of 0.1 μg.

Structural and properties' characterization

The crystallinity and microstructural analysis of the as-synthesized nanocomposite films were analyzed using X-ray diffractometer (XRD, Bede D1) and field emission transmission electron microscope (FE-TEM, JEOL JEM-2100F). Field emission scanning electron microscope (SEM, Hitachi SU8010) and EDS analyses were used to analyze surface morphology and elemental composition. X-ray photoelectron spectroscopy (XPS, ULVAC-PHI Quantera SXM) was utilized to examine the oxidation states of cobalt oxide/CNTs nanocomposite film. The specific surface area of the nanocomposite was determined by BET (Brunauer, Emmett, and Teller theory) surface area analyzer (ASAP2020). To investigate the thermal stability of the samples and to know the content of Co_3O_4 in the composites, thermogravimetric analysis (TGA) was performed from 50 to 950 °C with a ramping rate of 3 °C min^{-1} under air atmosphere using thermogravimetric analyzer (TGA, TA Instruments Q500).

Electrochemical testing

The electrochemical performances of the as-prepared Co_3O_4/CNTs nanocomposite electrodes were investigated in a three-electrode cell. Here, saturated calomel electrode (SCE) was used as a reference electrode, platinum sheet as a counter electrode, and nanocomposite film grown by EPD as a working electrode. All electrochemical measurements were carried out in a 1 M KOH aqueous electrolyte solution at ambient temperature. Cyclic voltammetry (CV),

galvanostatic charge/discharge cycling (GCD), and electrochemical impedance spectroscopy (EIS) were conducted using CH Instruments 618B electrochemical analyzer.

The specific capacitance (F g^{-1}) was calculated from CV curve according to Eq. (1):

$$C = \frac{\int_{E_i}^{E_f} I(E)\mathrm{d}E}{m \cdot v \cdot (E_f - E_i)}, \tag{1}$$

where m is the mass of active material, v is the scan rate, E_i and E_f, respectively, are the initial and the final voltages in the CV measurements, and $(E_f - E_i)$ is the potential window width.
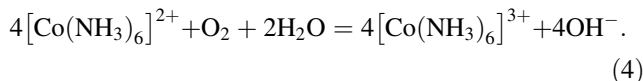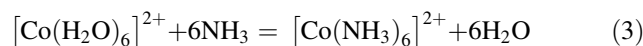
The specific capacitance (F g^{-1}) from GCD curve was calculated using the following equation:

$$C = \frac{I \cdot \Delta t}{\Delta V \cdot m}, \tag{2}$$

where I is the discharge current, Δt is the time for a full discharge, m is the mass of active material, and ΔV is the width of the potential window for a full discharge.

Results and discussion

It is known that after purification process of CNTs in 70 % HNO_3, a large number of oxygen-containing functional groups attached on the surface of CNTs which render CNT surface negatively charged. So, the cobalt cations in the solution are adsorbed on the surface of CNTs via electrostatic attraction and then transform into Co_3O_4. Cobalt nitrate ($[Co(H_2O)_6](NO_3)_2$ or $Co(NO_3)_2 \cdot 6H_2O$) consists of octahedral hexaaquacobalt (II) cations ($[Co(H_2O)_6]^{2+}$) and nitrate anions. In the presence of excess ammonia, NH_3 replaces water as a ligand to give hexaamminecobalt (II) ions ($[Co(NH_3)_6]^{2+}$), which rapidly oxidized to $[Co(NH_3)_6]^{3+}$ by O_2. The above-mentioned mechanism can be expressed by the following reactions [9]:

$$[Co(H_2O)_6]^{2+} + 6NH_3 = [Co(NH_3)_6]^{2+} + 6H_2O \tag{3}$$

$$4[Co(NH_3)_6]^{2+} + O_2 + 2H_2O = 4[Co(NH_3)_6]^{3+} + 4OH^-. \tag{4}$$

Then, under the hydrothermal conditions, $[Co(NH_3)_6]^{3+}$ decomposed at a certain temperature to yield spinel-like Co_3O_4 nanostructures [21].

Figure 1 shows the SEM images of the Co_3O_4/CNTs nanocomposites obtained at a certain temperature (180 °C) with different durations of hydrothermal process, in which the amount of $Co(NO_3)_2$ was kept constant (2 mmol) throughout the experiments. When the reaction time was 1 h, only few and small-sized individual Co_3O_4 nanoparticles could be formed on the surfaces of CNTs as shown in Fig. 1a. As the reaction time was extended to 4 h, the
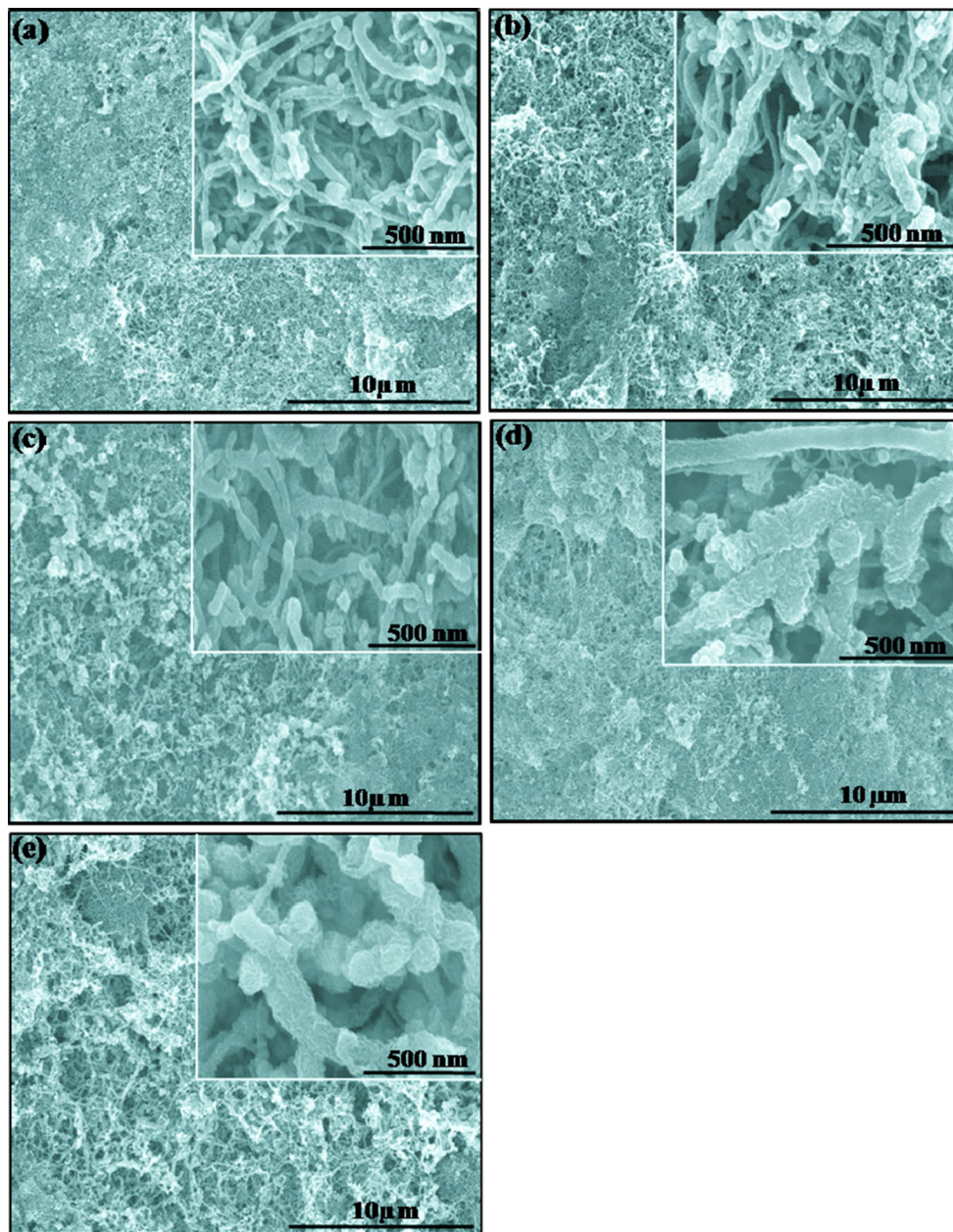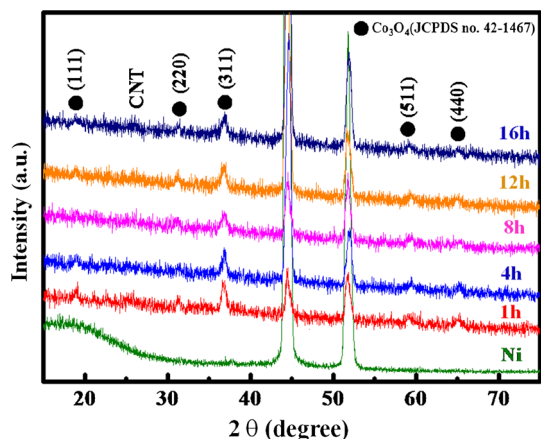
Fig. 1 SEM images of Co$_3$O$_4$/CNTs nanocomposites for fixed precursor concentration of 2 mmol at various hydrothermal reaction times: **a** 1 h, **b** 4 h, **c** 8 h, **d** 12 h, and **e** 16 h

individual Co$_3$O$_4$ nanoparticles start stacking together to form short-length nanorod-type structure on the surface of CNTs as shown in Fig. 1b. As the reaction time was increased to 8 h, the stacking increases and almost entire CNT surface was covered with a uniform layer of Co$_3$O$_4$ nanostructures (Fig. 1c). Upon further prolonging the reaction time, the thickness of Co$_3$O$_4$ layer over a CNT surface was increased as shown in Fig. 1d, e.

X-ray diffraction measurements were utilized to investigate the crystalline nature and structural properties of electrode materials synthesized at different hydrothermal reaction times of 1, 4, 8, 12, and 16 h, as shown in Fig. 2. With the exception of four typical peaks assigned to the CNT and Ni substrate at 26°, 44.47°, 51.8°, and 76.35°, five well-defined diffraction peaks were obtained at $2\theta \sim 19°$, 31°, 37°, 59°, and 65° that are representatives of (111), (220), (311), (511), and (440) planes of cubic Co$_3$O$_4$ phase (JCPDS, No. 42-1467), respectively. The average particle sizes of Co$_3$O$_4$ thin films were calculated using Debye–Scherrer formula (Eq. 5):

Fig. 2 X-ray diffraction patterns of Ni foil and electrodes composed of Co_3O_4/CNTs nanocomposite on Ni substrate for fixed $Co(NO_3)_2$ concentration of 2 mmol at various hydrothermal reaction times

$$D = \frac{C\lambda}{\beta \cos \theta} \tag{5}$$

where β is the full width at half maximum (FWHM) of X-ray peak in radians, λ is the X-ray wavelength (0.154 nm for Cu Kα radiation), C is the correction factor taken as 0.89, and D is the crystallite size. According to the Debye–Scherrer formula, FWHM is inversely proportional to the crystallite size, i.e., smaller particle size will be obtained for a sample with larger FWHM. In Fig. 2, the peak at $2\theta = 36.7°$ with hkl (311) for the electrode material prepared with a hydrothermal reaction time of 8 h was found to have the largest FWHM value (0.86°), indicating the smallest size (~ 9.32 nm) of cobalt oxide crystals among the five test samples. It has been generally accepted that the smaller particle size makes larger surface area and thus plays an essential role in the specific capacitance, which, being closely related to the surface reactions, depends on the surface area [22–24]. As a result, the electrode material prepared with a reaction time of 8 h, which was supposed to have the highest specific capacitance, would be further investigated by TGA and BET measurements.

TGA measurements were performed to know the thermal stability of the samples and to find out the content of Co_3O_4 in the samples. For TGA, samples were heated in air atmosphere at a ramp rate of 3 °C/min from 50 to 950 °C. Figure 3 shows the TGA curves of the Co_3O_4/CNTs nanocomposite obtained for a fixed cobalt nitrate concentration of 2 mmol at a hydrothermal time of 8 h. The first stage of weight loss within the temperature range of 50–150 °C can be attributed to the removal of surface-adsorbed water, and the second stage of weight loss within the temperature range of 180–260 °C is associated with the interlayered water evaporation. The third stage of weight loss between 180 and 300 °C can be ascribed to the decomposition of hydrophilic functional groups attached
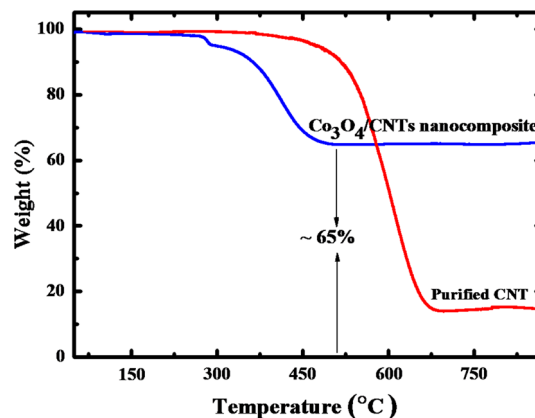
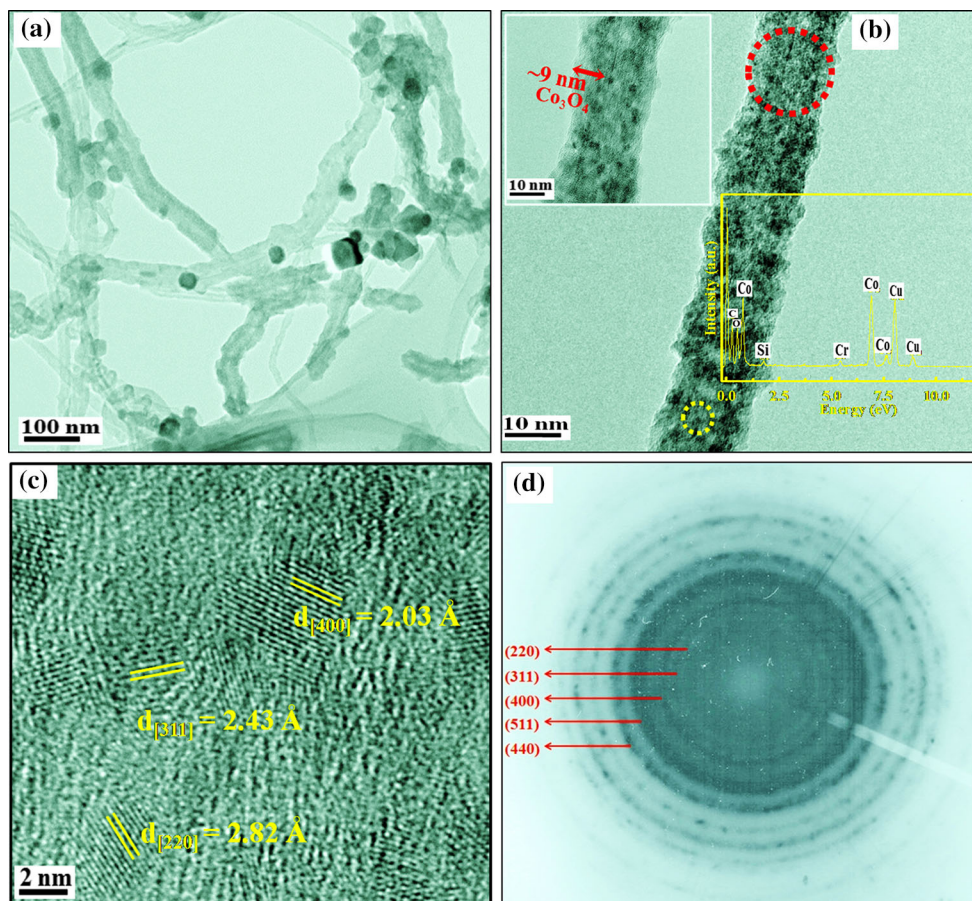**Fig. 3** Thermogravimetric analysis (TGA) curve of the electrode composed of Ni foil and Co_3O_4/CNTs nanocomposites prepared with 2 mmol $Co(NO_3)_2$ concentration and 8 h reaction time in hydrothermal process

with the CNT surface after acidic purification process [25, 26]. The additional weight loss between 350 and 600 °C corresponds to the oxidation of CNTs [27]. The plot demonstrates a total weight loss of 35 % indicating that the Co_3O_4 content in the Co_3O_4/CNTs is ~ 65 %.

More specific structural information about the nanocomposites can be obtained through TEM images as shown in Fig. 4. In Fig. 4a, the cobalt oxide nanoparticles were found to be uniformly decorated on the surface of CNTs. Besides, a layer was also seen to be coated on the surfaces of CNTs in Fig. 4b. The layer turned out to be composed of cobalt and oxygen elements, which was confirmed through EDS analysis. The inset in Fig. 4b shows that the average thickness of these Co_3O_4 layers in the nanocomposites is about 9 nm, which verifies the XRD results. HRTEM image, shown in Fig. 4c, reveals the polycrystalline nature of this layer on the surface of CNTs, consistent with the XRD results. Furthermore, the d-spacings in Fig. 4c were 2.43, 2.82, and 2.03 Å, which corresponds to the (311), (220), and (400) crystal planes of cubic phase of Co_3O_4, respectively. The selected-area electronic diffraction (SAED) ring pattern shown in the inset of Fig. 4d can also be indexed to the cubic phase of Co_3O_4. Thus, both TEM and XRD results suggest that the nanocomposites consist of crystalline Co_3O_4 nanostructure, which distributed on the surface of CNTs.

Figure 5 shows the nitrogen adsorption/desorption isotherm of the Co_3O_4/CNTs nanocomposite. The isotherm exhibits a significant hysteresis loop, indicating the existence of mesopores formed between particles. The specific surface area of Co_3O_4/CNTs nanocomposite is 92.2 m^2 g^{-1} which possesses a narrow mesoporous distribution at around 19–100 Å as shown in the inset of Fig. 5. Because the size range of the hydrated ions in the electrolyte is typically 6–7.6 Å, the pore size at the range of

Fig. 4 **a** Low- and **b** high-magnification TEM micrographs, **c** HRTEM image, and **d** SAED pattern of the Co_3O_4/CNTs nanocomposite synthesized with 2 mmol $Co(NO_3)_2$ concentration at a hydrothermal reaction time of 8 h
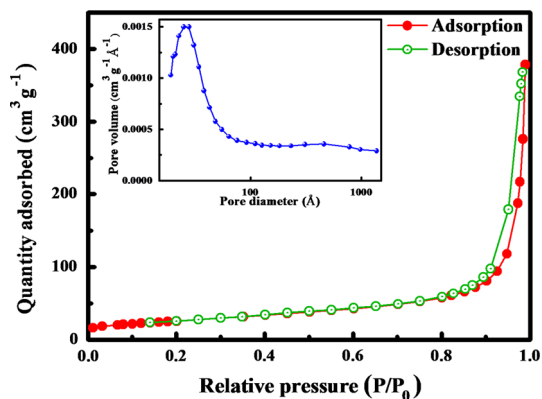

Fig. 5 N_2 adsorption–desorption isotherm and the pore size distribution curve of the Co_3O_4/CNTs nanocomposite prepared with 2 mmol $Co(NO_3)_2$ concentration and 8 h reaction time in hydrothermal process

8–50 Å seems to be an effective factor to enhance the specific capacitance [28].

In order to perform EPD process successfully, the nanocomposite particles in the IPA dispersion should be charged either positively or negatively by adding some suitable additives or surfactants in the dispersion. To synthesize nanocomposite material, we have utilized the functionalized MWCNTs, in which –OH and HO–C=O functional groups are attached with the CNT surface. These functional groups improve the dispersibility of CNTs in the solvent and affect the adsorption capacity onto the surface of CNTs. It has been reported that the electrical charge on the hydrated particles or functionalized CNTs' surface greatly depends on the pH of the solution. At lower (acidic) pH values, the surface is expected to have a net positive charge, while the surface charge changed from positive to negative as the pH increases [29–31]. In the present work, 37 % HCl has been used to adjust the pH of the solution and it acts as a surfactant to charge the surface of the nanocomposite particles. Based on the above discussion, the surface charging mechanism can be represented as

$$-COH_2^+ \xleftarrow{H+} -COH \xrightarrow{OH-} CO^- + H_2O.$$
(Low pH)   (High pH)
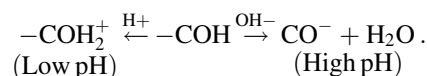
This mechanism describes the pH-dependent adsorption of protons or hydroxyls as charge-determining ions onto the

available surface sites of Co_3O_4/CNT nanocomposite. It explains why during EPD process Co_3O_4/CNT nanocomposite particles in the acidic dispersion move toward cathode (Ni sheet) and deposit on it to form binder-free electrode for supercapacitor.

The potential applications of the supercapacitors of the as-synthesized electrodes with various reaction times in the hydrothermal process were investigated through CV, galvanostatic charge–discharge (GCD), and electrical impedance spectroscopy (EIS) measurements in 1 M KOH electrolyte. From CV curves in Fig. 6a, there exist obvious redox peaks, due to the electrochemical charge transfer reactions $Co(II) \leftrightarrow Co(III) \leftrightarrow Co(IV)$, which reveal that charge storage of the Co_3O_4/CNTs/Ni electrode is a characteristic of the pseudocapacitive process originating from reversible redox reactions. The variation of measured specific capacitances of nanocomposites with different hydrothermal times is shown in the inset of Fig. 6a. The calculated specific capacitances for 1-, 4-, 8-, 12-, and 16-h samples at a scan rate of 100 mV s^{-1} are 562, 623, 686, 665, and 349 F g^{-1}, respectively.

In comparison with the CV results, Fig. 6d shows the charge/discharge (GCD) curves at the same current density of 3 A g^{-1} between -0.2 and 0.5 V in aqueous electrolyte (1 M KOH) at 25 °C. It also exhibits the characteristic of pseudocapacitor. In addition, the internal resistance (IR drop) in GCD curves has also been investigated. The IR drops for 1-, 4-, 8-, 12-, and 16-h samples are 0.8, 0.9, 0.88, 0.9, and 0.78 mV, respectively, and all of these are quite small in numbers. It can be seen that the GCD curve of 8-h sample is more symmetric than those of the others, which indicates the good reversible capability. The specific capacitance of 8-h sample at a current density of 3 A g^{-1} is 705 F g^{-1}, which is higher than those of 1-h (505 F g^{-1}), 4-h (554 F g^{-1}), 12-h(576 F g^{-1}), and 16-h (273 F g^{-1}) samples as shown in the inset of Fig. 6b.

Figure 6c shows a Nyquist plot from EIS for Co_3O_4/CNTs/Ni electrode samples obtained at various hydrothermal times. It reveals the characteristic features of the electron transfer between the electrolyte and the electrode surface. Determined from the point of intersection of the real axis in the range of high frequency, the internal resistance (R_s) of the electrode including the ionic resistance of electrolyte, the intrinsic resistance of the active material, and the contact resistance at the active material/
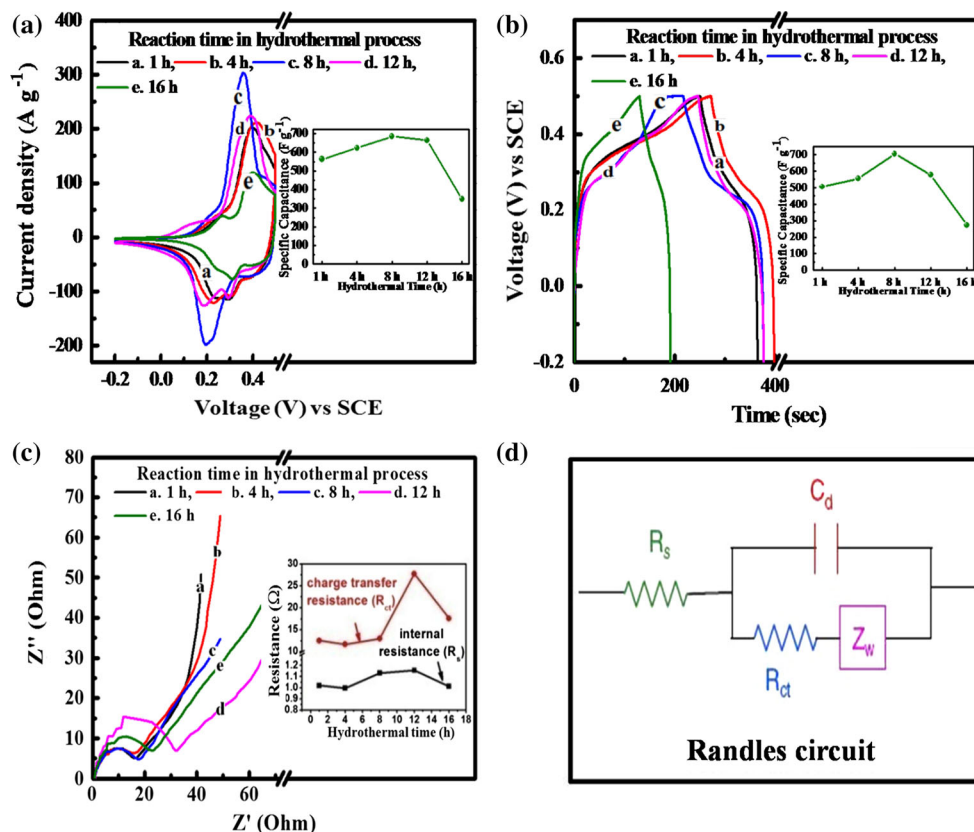
Fig. 6 **a** CV curves at a scan rate of 100 mV s^{-1} (the *inset* shows the specific capacitance calculated by CV curves), **b** GCD curves at a current density of 3 A g^{-1}; the *inset* represents the specific capacitance calculated by GCD curves, **c** Nyquist plots with different hydrothermal times for a fixed precursor concentration of 2 mmol [the *inset* shows the effect of hydrothermal reaction time on charge transfer resistance (R_{ct}) and internal resistance (R_s)], and **d** impedance function and typical equivalent circuit (Color figure online)

Table 1 The R_s and R_{ct} of Co_3O_4/CNTs nanocomposites at various hydrothermal reaction times for a fixed precursor concentration of 2 mmol

Reaction time (h)	1	4	8	12	16
Internal resistance, R_s (Ω)	1.01	1.00	1.13	1.16	1.01
Charge transfer resistance, R_{ct} (Ω)	12.53	11.68	12.98	27.76	17.6

current collector interface are about 1 Ω cm^2. Second, all spectra show a depressed semicircle from the high-frequency end to the middle-frequency region, attributed to the charge transfer resistance (R_{ct}) and double-layer capacitance at the electrode/electrolyte interface. The inset in Fig. 6c shows the effect of hydrothermal reaction times on charge transfer resistance (R_{ct}) and internal resistance (R_s)). The linear parts at lower frequencies correspond to the Warburg impedance, which is described as a diffusive resistance of the OH$^-$ ion within the porous electrode. The low-frequency end shows capacitive-like behavior. Such a pattern of the impedance spectra can be fitted very well with an equivalent circuit shown in Fig. 6d. Their R_s and R_{ct} can be fitted by the Zsimpwin software and are shown

in Table 1. The radius of semicircle declines when hydrothermal time is decreased, which implies that the thinner Co_3O_4 layer over CNTs makes the charge transfer easier.

To get more information about the electrochemical behavior and capacitor performance of Co_3O_4/CNTs/Ni electrode, we performed the detailed measurements of CV, GCD, and long-term stability test in a three-electrode configuration cell for the sample synthesized at 8 h hydrothermal reaction time. Figure 7a shows the CV curves with different scan rates between −0.2 and 0.5 V in aqueous electrolyte (1 M KOH) at 25 °C. It is observed that, as the scan rate decreases, the redox peaks become more prominent, signifying the slow faradaic reaction to
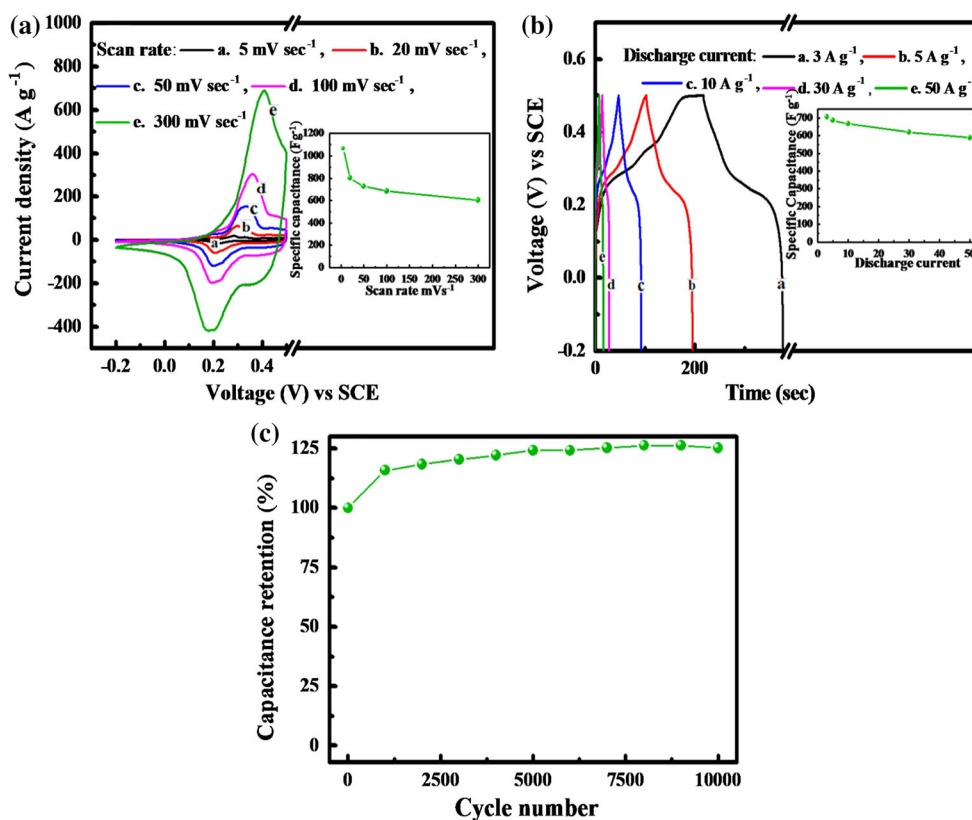
Fig. 7 **a** CV curves in 1 M KOH at scan rates of 5, 20, 50, 100, and 300 mV s^{-1}; the *inset* shows the summary plot of specific capacitance calculated from CV curves, **b** GCD curves in 1 M KOH at a current density of 3, 5, 10, 30, and 50 A g^{-1} (the *inset* shows the specific capacitance calculated from GCD curves, and **c** cycling stability (at a constant charge/discharge current density of 30 A g^{-1}) of the synthesized Co_3O_4/CNTs nanocomposite at a fixed precursor concentration of 2 mmol and a hydrothermal reaction time of 8 h (Color figure online)

occur predominantly at low scan rates. It is noteworthy that the redox peaks shift as the scan rate increases, which is attributed to the resistance of the electrode [32]. The variation of measured specific capacitances with different scan rates is shown in the inset of Fig. 7a. The calculated specific capacitances are 1066, 802, 727, 686, and 603 F g^{-1} at different scan rates of 5, 20, 50, 100, and 300 mV s^{-1}, respectively.

Figure 7b depicts the charge/discharge behavior between −0.2 and 0.5 V at various current densities. It also exhibits the characteristic of pseudocapacitor. Moreover, no obvious distortions in the GCD curves were observed as the current density increased, suggesting that the Co$_3$O$_4$/CNTs/Ni electrode is well tolerant. From the GCD curve, the specific capacitances at current densities of 3, 5, 10, 30, and 50 A g^{-1} come out to be 705, 686, 666, 619, and 589 F g^{-1}, respectively, as shown in the inset of Fig. 7b. Under a larger current density, nearly 84 % of the initial value was maintained, which implies that Co$_3$O$_4$/CNTs/Ni electrode has a good rate capability.

Figure 7c displays the cycling stability of the Co$_3$O$_4$/CNTs/Ni electrode pseudocapacitor with the 1 M KOH electrolyte at a constant charge/discharge current density of 30 A g^{-1}. The long-term cycling test is one of the important parameters for evaluating the performance of a supercapacitor. In contrast with most cycle stability tests in the literature, here we observed that the capacitance retention gradually increases with an increase in the cycle number till 8,000 charge/discharge cycles, where it is about 125 % of the initial value. This phenomenon is termed electro-activation [33]. It implies that there exists an activation process for the faradaic pseudocapacitance of Co$_3$O$_4$/CNT nanocomposite electrode, which makes it completely activated via the intercalation and deintercalation of ions. This electro-activation increases the active sites inside the electrode material and as a result increases the specific capacitance [34, 35]. After 10,000 charge/discharge cycles, the capacitance retention still remains high, indicating the excellent cycle durability of the pseudocapacitor.

Not only high capacitance obtained but also long cycling stability of the synthesized Co$_3$O$_4$/CNTs nanocomposite for fixed cobalt nitrate concentration of 2 mmol at a hydrothermal reaction time of 8 h is mainly attributed to the synergistic effects of Co$_3$O$_4$ and CNTs. The Co$_3$O$_4$/CNTs nanocomposites possess high structural stability, high specific surface area, appropriate morphology with smaller particle size, and narrow mesoporous distribution for short path lengths of ion diffusion and electron transport. The mesopore size distribution existing in the nanocomposite material can sever as a robust reservoir for ions, and also greatly enhances the diffusion kinetics within the electrode.

Conclusions

In summary, Co$_3$O$_4$/CNTs nanocomposites have been successfully synthesized and coated on Ni substrate using a hydrothermal method combined with EPD method. These methods offer several significant advantages, like room-temperature processing, good control ability, low cost, and additive-free electrode fabrication, over other synthesis and electrode fabrication methods.

It has been shown that the hydrothermal reaction time has a significant influence on the hydrolysis rate, the nucleation as well as crystal growth processes. The XRD and TEM analyses show that the spinal phase Co$_3$O$_4$ has been synthesized in our work, while BET measurement exhibits the surface area of 92.2 m^2 g^{-1} and a narrow mesoporous distribution at around 19–100 Å.

The obtained porous structure Co$_3$O$_4$/CNTs nanocomposites synthesized using a fixed cobalt nitrate concentration of 2 mmol at a hydrothermal time of 8 h exhibits high specific capacitance (705 F g^{-1} at a current density of 3 A g^{-1}), fast rate capability, well tolerance, and excellent cycling stability (∼125 % capacitance retention after 10,000 charge/discharge cycles) attributed to the effective distributions of the pore size, high specific surface area, and the appropriate morphology with smaller particle size. These results indicate that our designed Co$_3$O$_4$/CNTs nanocomposites' pseudocapacitor is appropriate for practical applications.

References

1. Sevilla M, Mokaya R (2014) Energy storage applications of activated carbons: supercapacitors and hydrogen storage. Energy Environ Sci 7:1250–1280
2. Abruna HD, Kiya Y, Henderson JC (2008) Batteries and electrochemical capacitors. Phys Today 61:43–47
3. Wang Y, Xia Y (2013) Recent progress in supercapacitors: from materials design to system construction. Adv Mater 25:5336–5342
4. Conway BE, Pell WG (2003) Double-layer and pseudocapacitance types of electrochemical capacitors and their applications to the development of hybrid devices. J Solid State Electrochem 7:637–644
5. Wei H, Zhu J, Wu S et al (2013) Electrochromic polyaniline/graphite oxide nanocomposites with endured electrochemical energy storage. Polymer 54:1820–1831
6. Li Z, Zhou Z, Yun G et al (2013) High-performance solid-state supercapacitors based on graphene-ZnO hybrid nanocomposites. Nanoscale Res Lett 8:473
7. Arabale G, Wagh D, Kulkarni M et al (2003) Enhanced supercapacitance of multiwalled carbon nanotubes functionalized with ruthenium oxide. Chem Phys Lett 376:207–213

8. Zhou R, Meng C, Zhu F et al (2010) High-performance super-capacitors using a nanoporous current collector made from super-aligned carbon nanotubes. Nanotechnology 21:345701–345707

9. Xiong S, Yuan C, Zhang X et al (2009) Controllable synthesis of mesoporous Co_3O_4 nanostructures with tunable morphology for application in supercapacitors. Chemistry 15:5320–5326

10. Sivakkumar SR, Ko JM, Kim DK et al (2007) Performance evaluation of CNT/polypyrrole/MnO_2 composite electrodes for electrochemical capacitors. Electrochim Acta 52:7377–7385

11. Li QY, Li ZS, Lin L et al (2010) Facile synthesis of activated carbon/carbon nanotubes compound for supercapacitor application. Chem Eng J 156:500–504

12. Hung CJ, Hung JH, Lin P, Tseng TY (2011) Electrophoretic fabrication and characterizations of manganese oxide/carbon nanotube nanocomposite pseudocapacitors. J Electrochem Soc 158:A942–A947

13. Adekunle AS, Ozoemena KI, Agboola BO (2013) MWCNTs/metal (Ni Co, Fe) oxide nanocomposite as potential material for supercapacitors application in acidic and neutral media. J Solid State Electrochem 17:1311–1320

14. Fisher RA, Watt MR, Ready WJ (2013) Functionalized carbon nanotube supercapacitor electrodes: a review on pseudocapacitive materials. ECS J Solid State Sci Technol 2(10):M3170–M3177

15. Abdolmaleki A, Kazerooni H, Gholivand MB et al (2015) Facile electrostatic coprecipitation of f-SWCNT/Co_3O_4 nanocomposite as supercapacitor material. Ionics 21:515–523

16. Guan C, Qian X, Wang X et al (2015) Atomic layer deposition of Co_3O_4 on carbon nanotubes/carbon cloth for high-capacitance and ultrastable supercapacitor electrode. Nanotechnology 26:094001–094007

17. Lu W, Hartman R, Qu L, Dai L (2011) Nanocomposite electrodes for high-performance supercapacitors. J Phys Chem Lett 2:655–660

18. Yuksel R, Sarioba Z, Cirpan A et al (2014) Transparent and flexible supercapacitors with single walled carbon nanotube thin film electrodes. ACS Appl Mater Interfaces 6:15434–15439

19. Wang S, Dryfe RAW (2013) Graphene oxide-assisted deposition of carbon nanotubes on carbon cloth as advanced binder-free electrodes for flexible supercapacitors. J Mater Chem A 1:5279–5283

20. Hung CJ, Lin P, Tseng TY (2013) Electrophoretic fabrication and pseudocapacitive properties of graphene/manganese oxide/carbon nanotube nanocomposites. J Power Sources 243:594–602

21. Farhadi S, Pourzare K (2012) Simple and low temperature preparation of Co_3O_4 sphere-like nanoparticles via solid-state thermolysis of the $[Co(NH_3)_6](NO_3)_3$ complex. Mater Res Bull 47:1550–1556

22. Gaber A, Abdel-Rahim MA, Abdel-Latief AY et al (2014) Influence of calcination temperature on the structure and porosity of nanocrystalline SnO_2 synthesized by a conventional precipitation method. Int J Electrochem Sci 9:81–95

23. Lee G, Varanasi CV, Liu J et al (2015) Effects of morphology and chemical doping on electrochemical properties of metal hydroxides in pseudocapacitors. Nanoscale 7:3181–3188

24. Kondrat S, Wu P, Qiao R, Kornyshev AA (2014) Accelerating charging dynamics in subnanometre pores. Nat Mater 13:387–393

25. Lv M, Liu K, Li Y et al (2014) Facile synthesis of Co_3O_4/mildly oxidized multiwalled carbon nanotubes/reduced mildly oxidized graphene oxide ternary composite as the material for supercapacitors. Bull Korean Chem Soc 35:1349–1355

26. Singh BP, Singh D, Mathur RB et al (2008) Influence of surface modified MWCNTs on the mechanical, electrical and thermal properties of polyimide nanocomposites. Nanoscale Res Lett 3:444–453

27. Zhuo L, Wu Y, Ming J et al (2013) Facile synthesis of a Co_3O_4–carbon nanotube composite and its superior performance as an anode material for Li-ion batteries. J Mater Chem A 1:1141–1147

28. Cao L, Lu M, Li HL (2005) Preparation of mesoporous nanocrystalline Co_3O_4 and its applicability of porosity to the formation of electrochemical capacitance. J Electrochem Soc 152:A871–A875

29. Atieh MA, Bakather OY, Tawbini BA et al (2010) Effect of carboxylic functional group functionalized on carbon nanotubes surface on the removal of lead from water. Bioinorg Chem Appl 603978:1–9

30. Wang G, Sarkar P, Nicholson PS (1997) Influence of acidity on the electrostatic stability of alumina suspensions in ethanol. J Am Ceram Soc 80:965–972

31. Simate GS, Iyuke SE, Ndlovu S et al (2012) The heterogeneous coagulation and flocculation of brewery waste water using carbon nanotubes. Water Res 46:1185–1197

32. Ghosh D, Giri S, Das CK (2013) Preparation of CTAB-assisted hexagonal platelet $Co(OH)_2$/graphene hybrid composite as efficient supercapacitor electrode material. ACS Sustain Chem Eng 1:1135–1142

33. Cheng Q, Tang J, Ma J et al (2011) Graphene and nanostructured MnO_2 composite electrodes for supercapacitors. Carbon 49:2917–2925

34. Zhu L, Wu W, Zhu Y et al (2015) Composite of CoOOH nanoplates with multiwalled carbon nanotubes as superior cathode material for supercapacitors. J Phys Chem C 119:7069–7075

35. Rakhi RB, Chen W, Cha D (2012) Substrate dependent self-organization of mesoporous cobalt oxide nanowires with remarkable pseudocapacitance. Nano Lett 12:2559–2567